Mathematical Modelling in Photo-Acoustic Imaging*

Habib Ammari† Emmanuel Bossy† Vincent Jugnon‡
Hyeonbae Kang§

July 22, 2009

Abstract

This paper is devoted to mathematical modelling in photo-acoustic imaging. We propose a new method for reconstructing absorbing regions inside a bounded domain from boundary measurements of the induced acoustic signal. We also show the focusing property of the back-propagated acoustic signal. Indeed, we provide two different methods for locating a targeted optical absorber from boundary measurements of the induced acoustic signal. The first method consists of a MUltiple Signal Classification (MUSIC) type algorithm and the second one uses a multi-frequency approach. We also show results of computational experiments to demonstrate efficiency of the algorithms.

AMS subject classifications. 31B20, 35B37,35L05

Key words. photo-acoustic imaging, wave equation, asymptotic expansion, reconstruction algorithm, MUSIC algorithm, multi-frequency imaging approach, optical tomography

1 Introduction

The photo-acoustic effect is the physical basis for photo-acoustic imaging; it refers to the generation of acoustic waves by the absorption of optical energy [26, 15]. In photo-acoustic imaging, energy absorption causes thermo-elastic expansion of the tissue, which in turn leads to propagation of a pressure wave. This signal is measured by transducers distributed on the boundary of the object, which is in turn used for imaging optical properties of the object.

*This work was partially supported by the ANR project EchoScan (AN-06-Blan-0089), ANR PAG-HIFU (JC07-195015), the grant KOSEF R01-2006-000-10002-0, the STAR project 190117RD, and KICOS project K20803000001-08B1200-00110.

†Institut Langevin, ESPCI ParisTech, CNRS UMR 7587, 10 rue Vauquelin, 75231 Paris Cedex 05, France (habib.ammari@espci.fr, emmanuel.bossy@espci.fr).

‡Centre de Mathématiques Appliquées, CNRS UMR 7641, Ecole Polytechnique, 91128 Palaiseau, France (jugnon@cmap.polytechnique.fr).

§Department of Mathematics, Inha University, Incheon 402-751, Korea (hbkang@inha.ac.kr).

In the last decade or so, work on photo-acoustic imaging in biomedical applications has come a long way. The motivation is to combine ultrasonic resolution with high contrast due to optical absorption. In pure optical imaging, optical scattering in soft tissues degrades spatial resolution significantly with depth. Pure optical imaging is very sensitive to optical absorption but can only provide a spatial resolution of the order of 1 cm at cm depths. Pure conventional ultrasound imaging is based on the detection of the mechanical properties (acoustic impedance) in biological soft tissues. It can provide good spatial resolution because of its millimetric wavelength and weak scattering at MHz frequencies. The significance of photo-acoustic imaging combines both approaches to provide images of *optical* contrasts (based on the optical absorption) with the *ultrasound* resolution.

If the medium is acoustically homogeneous and has the same acoustic properties as the free space, then the boundary of the object plays no role and the optical properties of the medium can be extracted from measurements of the pressure wave by inverting a spherical Radon transform (see the next section for references for reconstruction in the free space) [2, 22]. In the more realistic situation, where a boundary condition has to be imposed on the pressure field, such an inversion formula does not hold. In this paper, we propose a new approach for reconstructing absorbing regions and absorbing energy density inside a bounded domain from boundary data. We also consider a problem of selective detection which is to locate a targeted optical absorber among several absorbers from boundary measurements of the induced acoustic signal.

We first consider a problem of identifying absorbing regions from boundary measurements. It turns out that the spherical waves centered at some points, which we call probe waves, may serve as solutions to adjoint problems to the wave equation for the photo-acoustic phenomena. By integrating the boundary measurements against this spherical wave, we can estimate the duration of the wave on the absorber. Then by choosing a few waves centered at different points and taking intersection of durations of these waves we can estimate the location and size of the absorber pretty accurately.

We then turn our attention to the selective detection and propose two methods to localize the targeted absorber. The first method is based on a MUltiple SIgnal Classification (MUSIC) type algorithm in conjunction with the time reversal technique, namely, back-propagation of the acoustic signal [12, 13, 14, 4]. This method works when the absorbing coefficient of the targeted absorber is in contrast with those of other absorbers. We also investigate the focusing property of the back-propagated acoustic signal. An alternative method of selective detection is based on the fact that the absorbing coefficient may vary depending on the frequencies. Some absorbers are transparent at certain frequency while they are quite absorbing at other frequencies. This phenomenon make a multi-frequency approach work to detect a targeted absorber. We propose a detailed process of this multi-frequency approach.

These methods are tested numerically using simulation data. Computational results clearly exhibit their accuracy and efficiency. It should be emphasized that all the methods proposed in this paper are derived using approximations which are valid under the assumption that the optical absorbers are of small size.

The paper is organized as follows: In section 2, we formulate the mathematical problems (in a bounded domain) and review known results of reconstruction using the spherical Radon transform in the free space. In section 3 we propose a reconstruction method using probe waves. Section 4 is to investigate the focusing property of the back-projected signal. Section 5 is devoted to the selective detection. Section 6 is to present results of computational experiments. The paper ends with a short discussion.

2 Mathematical Formulation

Let $D_l, l = 1, \ldots, m$, be m absorbing domains inside the non-absorbing background bounded medium $\Omega \subset \mathbb{R}^d, d = 2$ or 3. In an acoustically homogeneous medium, the photo-acoustic effect is described by the following equation:

$$\frac{\partial^2 p}{\partial t^2}(x,t) - c^2 \Delta p(x,t) = \gamma \frac{\partial H}{\partial t}(x,t), \quad x \in \Omega, \quad t \in]-\infty, +\infty[, \tag{2.1}$$

where c is the acoustic speed in Ω, γ the dimensionless Grüneisen coefficient in Ω, and $H(x,t)$ a heat source function (absorbed energy per unit time per unit volume).

Assuming the stress-confinement condition, the source term can be modelled as $\gamma H(x,t) = \delta(t) \sum_l \chi_{D_l}(x) A_l(x)$. Here and throughout this paper χ_{D_l} is the indicator function of D_l. Under this assumption, the pressure in an acoustically homogeneous medium obeys the following wave equation:

$$\frac{\partial^2 p}{\partial t^2}(x,t) - c^2 \Delta p(x,t) = 0, \quad x \in \Omega, \quad t \in]0, T[, \tag{2.2}$$

for some final observation time T. The pressure satisfies either the Dirichlet or the Neumann boundary condition

$$p = 0 \quad \text{or} \quad \frac{\partial p}{\partial \nu} = 0 \quad \text{on } \partial\Omega \times]0, T[\tag{2.3}$$

and the initial conditions

$$p|_{t=0} = \sum_{l=1}^{m} \chi_{D_l}(x) A_l(x) \quad \text{and} \quad \left.\frac{\partial p}{\partial t}\right|_{t=0} = 0 \quad \text{in } \Omega. \tag{2.4}$$

Here and throughout this paper, ν denotes the outward normal to $\partial\Omega$. It is worth emphasizing that both the Dirichlet and Neumann boundary conditions in (2.3) yield good mathematical models in practice.

The inverse problem in photo-acoustic imaging is to determine the supports of nonzero optical absorption (D_l, $l = 1, \ldots, m$) in Ω and the absorbed optical energy density times the Grüneisen coefficient $A(x) = \sum_{l=1}^m A_l(x)\chi_{D_l}(x)$ from boundary measurements of $\frac{\partial p}{\partial \nu}$ on $\partial\Omega\times]0,T[$ if p satisfies the Dirichlet boundary condition and p on $\partial\Omega\times]0,T[$ if p satisfies the Neumann boundary condition. We will assume that T is large enough so that

$$T > \frac{\mathrm{diam}(\Omega)}{c}. \tag{2.5}$$

It says that the observation time is long enough for the wave initiated inside Ω to reach the boundary $\partial\Omega$.

The density $A(x)$ is related to the optical absorption coefficient distribution $\mu_a(x) = \sum_{l=1}^m \mu_l(x)\chi_{D_l}(x)$ by the equation $A(x) = \gamma\mu_a(x)\Phi(x)$, where Φ is the light fluence. The function Φ depends on the distribution of scattering and absorption within Ω, as well as the light sources. The reconstruction of the optical absorption coefficient distribution $\mu_a(x)$ from $A(x)$ is therefore a non-trivial task, out of the scope of this paper.

To date, photo-acoustic imaging has been restricted to the reconstruction of $A(x)$ from pressure measurements. The difficulty of reconstructing the absorbed optical energy density $A(x)$ from pressure boundary measurements on $\partial\Omega\times]0,T[$ comes from the boundary itself. Suppose $d = 3$ and consider the wave equation

$$\frac{\partial^2 p}{\partial t^2}(x,t) - c^2\Delta p(x,t) = 0$$

in the free space with the initial conditions $p = \sum_{l=1}^m \chi_{D_l}A_l(x)$ and $\partial_t p = 0$ at $t = 0$. The pressure p in this case can be written explicitly as follows:

$$p(x,t) = \frac{d}{dt}\left[\sum_{l=1}^m \int_{|x-x'|=ct} \frac{\chi_{D_l}(x')A_l(x')}{4\pi|x-x'|}\, dS(x')\right],$$

or equivalently,

$$p(x,t) = \frac{c}{4\pi}\frac{d}{dt}\left[t\sum_{l=1}^m \int_{|x'|=1} \chi_{D_l}(x+ctx')A_l(x+ctx')\, dS(x')\right], \tag{2.6}$$

where dS is the surface area element on the unit sphere, since $c^2t^2dS(x') = d\sigma(x')$. Formula (2.6) says that $c^{-1}t^{-1}\int_0^t p(x,\tau)d\tau$ is the spherical Radon transform of $A(x)$. Hence, we can reconstruct A by inverting the spherical Radon transform. We refer the reader to the papers [1, 2, 21, 27, 18, 19, 3] for uniqueness of the reconstruction and back-projection inversion procedures. See also [22].

In a bounded domain, there is no analogous to the representation formula (2.6) and very little is known in the literature. Only the half-space problem has been considered [25].

The main purpose of this paper is to deal with this difficulty and to develop new methods to reconstruct absorbing regions and their densities. We propose a method related to the time-reversal technique [14] for reconstructing A. We will also show the focusing property of the back-propagated acoustic signal and provide two different methods for locating a targeted optical absorber from boundary measurements of the induced acoustic signal. The first method consists of a MUSIC-type algorithm while the second one uses a multi-frequency approach. It is worth mentioning, in connection with our reconstruction methods, the nice analysis of the sensitivity of a photo-acoustic wave to the presence of small absorbing objects in [15].

3 A Reconstruction Method

The algorithms available in the literature are limited to unbounded media. They use the inversion of the spherical Radon transform. However, since the pressure field p is significantly affected by the acoustic boundary conditions at the tissue-air interface, where the pressure must vanish, we cannot base photo-acoustic imaging on pressure measurements made over a free surface. Instead, we propose the following algorithm.

Let v satisfy

$$\frac{\partial^2 v}{\partial t^2} - c^2 \Delta v = 0 \quad \text{in } \Omega \times]0, T[, \tag{3.1}$$

with the final conditions

$$v|_{t=T} = \frac{\partial v}{\partial t}\Big|_{t=T} = 0 \quad \text{in } \Omega, \tag{3.2}$$

which is an adjoint problem to (2.2)-(2.4). We will refer to v as a probe function or a probe wave.

Multiply both sides of (2.2) by v and integrate them over $\Omega \times [0, T]$. After some integrations by parts this leads to the following identity:

$$\int_0^T \int_{\partial\Omega} \frac{\partial p}{\partial \nu}(x,t) v(x,t)\, d\sigma(x)\, dt = \frac{1}{c^2} \sum_{l=1}^{m} \int_{D_l} A_l(x) \partial_t v(x,0) dx. \tag{3.3}$$

Here we assume that p satisfies the Dirichlet boundary condition.

Suppose first that $d = 3$. For $y \in \mathbb{R}^3 \setminus \overline{\Omega}$, let

$$v_y(x,t;\tau) := \frac{\delta\left(t + \tau - \frac{|x-y|}{c}\right)}{4\pi|x-y|} \quad \text{in } \Omega \times]0, T[, \tag{3.4}$$

where δ is the Dirac mass at 0 and $\tau > \frac{\text{dist}(y,\partial\Omega)}{c}$ is a parameter. It is easy to check that v_y satisfies (3.1) (see e.g. [17, page 117]). Moreover, since

$$|x - y| \leq \text{diam}(\Omega) + \text{dist}(y, \partial\Omega)$$

for all $x \in \Omega$, v_y satisfies (3.2) provided that the condition (2.5) is fulfilled.

We write

$$D_l = z_l + \epsilon B_l,$$

where z_l is the "center" of D_l, B_l contains the origin and plays a role of a reference domain, and ϵ is the common order of magnitude of the diameters of the D_l. Throughout this paper, we assume that z_l's are well-separated, *i.e.*,

$$|z_i - z_j| > C_0 \quad \forall i \neq j \tag{3.5}$$

for some positive constant C_0. Suppose that

$$A_l(x) = \sum_{|j|=0}^{N} \frac{1}{j!} a_j^{(l)} \cdot (x - z_l)^j \tag{3.6}$$

which is reasonable as D_l is small. Here, $j = (j_1, \ldots, j_d)$, $x^j = x_1^{j_1} \ldots x_d^{j_d}$, and $j! = j_1! \ldots j_d!$. Equation (3.6) corresponds to a multipolar expansion up to order N of the optical effect of D_l.

Choosing v_y as a probe function in (3.3), we obtain the new identity

$$\frac{1}{c^2} \sum_{l=1}^{m} \sum_{|j|=0}^{N} \frac{1}{j!} a_j^{(l)} \int_{D_l} (x - z_l)^j \partial_t v_y(x, 0; \tau) dx = \int_0^T \int_{\partial\Omega} \frac{\partial p}{\partial \nu}(x, t) v_y(x, t; \tau)\, d\sigma(x)\, dt. \tag{3.7}$$

Determination of location. Suppose for simplicity that there is only one absorbing object ($m = 1$) which we denote by $D(= z + \epsilon B)$. Identity (3.7) shows that

$$\tau \mapsto \int_0^T \int_{\partial\Omega} \frac{\partial p}{\partial \nu}(x, t) v_y(x, t; \tau)\, d\sigma(x)\, dt \tag{3.8}$$

is nonzero only on the interval $]\tau_a, \tau_e[$, where $\tau_a = \mathrm{dist}(y, D)/c$ is the first τ for which the sphere of center y and radius τ hits D and τ_e is the last τ for which such sphere hits D. This gives a simple way to detect the location (by changing the source point y and taking intersection of spheres). The quantity $\int_0^T \int_{\partial\Omega} \frac{\partial p}{\partial \nu}(x, t) v_y(x, t; \tau)\, d\sigma(x)\, dt$ can be used to probe the medium as a function of τ and y. For fixed y, it is a one-dimensional function. It is related to time-reversal in the sense that it is a convolution with a reversed wave.

Let us now compute $\int_D (x - z)^j \partial_t v_y(x, 0; \tau) dx$ for $\tau \in]\tau_a, \tau_e[$. Note that, in a distributional sense,

$$\partial_t v_y(x, 0; \tau) = \frac{\delta'\left(\tau - \frac{|x-y|}{c}\right)}{4\pi |x - y|}. \tag{3.9}$$

Thus we have

$$\int_D (x-z)^j \partial_t v_y(x,0;\tau)dx = \int_D \frac{(x-z)^j}{4\pi|x-y|}\,\delta'\left(\tau - \frac{|x-y|}{c}\right)dx.$$

Letting $s = |x-y|$ and $\sigma = \frac{x-y}{|x-y|}$, we get by a change of variables

$$\int_D (x-z)^j \partial_t v_y(x,0;\tau)dx = \frac{1}{4\pi}\int_0^{+\infty} s \int_{S^2} \chi_D(s\sigma+y)(s\sigma+y-z)^j \delta'(\tau - \frac{s}{c})\, ds\, d\sigma, \tag{3.10}$$

where S^2 is the unit sphere.

Define for multi-indices j

$$b_j(D,t;\tau) = \int_{S^2} \chi_D(c(\tau-t)\sigma+y)(c(\tau-t)\sigma+y-z)^j d\sigma.$$

Note that the function $b_j(D,t;\tau)$ is dependent on the shape of D (b_j is kind of moment of order j of the domain D). If we take D to be a sphere of radius r (its center is z), then one can compute $b_j(D,t;\tau)$ explicitly using the spherical coordinates.

Since

$$\int_0^{+\infty} s \int_{S^2} \chi_D(s\sigma+y)(s\sigma+y-z)^j \delta'(\tau-\frac{s}{c})\, ds\, d\sigma = -c^2 \frac{d}{dt}\Big[(\tau-t)b_j(D,t;\tau)\Big]\Big|_{t=0},$$

it follows from (3.10) that

$$\int_D (x-z)^j \partial_t v_y(x,0;\tau)dx = \frac{c^2}{4\pi}(b_j(D,0;\tau) - \tau b_j'(D,0;\tau)),$$

where b_j' is the derivative with respect to t. We then obtain the following theorem from (3.7).

Theorem 3.1 *For $\tau \in]\tau_a, \tau_e[$,*

$$\frac{1}{4\pi}\sum_{|j|=0}^{N} \frac{a_j}{j!}\cdot(b_j(D,0;\tau) - \tau b_j'(D,0;\tau)) = \int_0^T \int_{\partial\Omega} \frac{\partial p}{\partial \nu}(x,t) v_y(x,t;\tau)\, d\sigma(x)\, dt. \tag{3.11}$$

If the Dirichlet boundary condition (2.3) is replaced by the Neumann boundary condition:

$$\frac{\partial p}{\partial \nu} = 0 \quad \text{on } \partial\Omega\times]0,T[, \tag{3.12}$$

then (3.11) should be replaced by

$$\frac{1}{4\pi}\sum_{|j|=0}^{N} \frac{a_j}{j!}\cdot(b_j(D,0;\tau) - \tau b_j'(D,0;\tau)) = -\int_0^T \int_{\partial\Omega} \frac{\partial v_y}{\partial \nu}(x,t;\tau) p(x,t)\, d\sigma(x)\, dt. \tag{3.13}$$

Estimation of absorbing energy. Now, we show how to use formula (3.11) for estimating $a^{(j)}$ and some geometric features of D when the location z of D has been determined by the variations of the function in (3.8). Suppose that $N = 0$, *i.e.*, A is constant on D. Then (3.11) reads

$$\frac{1}{4\pi} a_0 \cdot (b_0(D,0;\tau) - \tau b_0'(D,0;\tau)) = \int_0^T \int_{\partial\Omega} \frac{\partial p}{\partial \nu}(x,t) v_y(x,t;\tau)\, d\sigma(x)\, dt.$$

Note that $b_0(D,0;\tau) - \tau b_0'(D,0;\tau)$ for $\tau > 0$ is supported in $[\tau_a, \tau_e]$. We then have

$$\begin{aligned} &\frac{|a_0|}{4\pi} \cdot \int_{\tau_a}^{\tau_e} \left| b_0(D,0;\tau) - \tau b_0'(D,0;\tau) \right| d\tau \\ &= \int_{\tau_a}^{\tau_e} \left| \int_0^T \int_{\partial\Omega} \frac{\partial p}{\partial \nu}(x,t) v_y(x,t;\tau)\, d\sigma(x)\, dt \right| d\tau. \end{aligned} \tag{3.14}$$

If we further assume that $D = z + \epsilon B$ for small ϵ and a sphere B of radius 1, then we can compute $b_0(D,t;\tau)$ explicitly. In fact, one can show that

$$b_0(D,t,\tau) = \begin{cases} \pi \dfrac{\epsilon^2 - (|z-y| - c|\tau - t|)^2}{c|z-y||\tau - t|} & \text{if } -\epsilon < |z-y| - c|\tau - t| < \epsilon, \\ 0 & \text{otherwise,} \end{cases} \tag{3.15}$$

and hence we deduce $c\tau_a = |z-y| - \epsilon$, $c\tau_e = |z-y| + \epsilon$, and

$$b_0(D,0,\tau) - \tau b_0'(D,0,\tau) = \frac{2\pi(|z-y| - c\tau)}{|z-y|}$$

for $\tau > 0$. Therefore, easy computations show that

$$|a_0|\epsilon^2 \approx c|z-y| \int_{\tau_a}^{\tau_e} \left| \int_0^T \int_{\partial\Omega} \frac{\partial p}{\partial \nu}(x,t) v_y(x,t;\tau)\, d\sigma(x)\, dt \right| d\tau, \tag{3.16}$$

which gives an approximation of $|a_0|\epsilon^2$. Higher-order approximations can be obtained from (3.11) as well.

Suppose now $d = 2$. Due to the two-dimensional nature of the Green function, we shall rather consider a new probe wave given by

$$v_\theta(x,t;\tau) = \delta\left(t + \tau - \frac{\langle x, \theta \rangle}{c}\right) \tag{3.17}$$

where $\theta \in S^1$, $\langle \cdot, \cdot \rangle$ denotes the Euclidian scalar product, and τ is a parameter satisfying

$$\tau > \max_{x \in \Omega} \left(\frac{\langle x, \theta \rangle}{c} \right).$$

We can still use the function

$$\tau \mapsto \int_0^T \int_{\partial\Omega} \frac{\partial p}{\partial \nu}(x,t) v_\theta(x,t;\tau)\, d\sigma(x)\, dt$$

to probe the medium as a function of τ. This quantity is non-zero on the interval $]\tau_a, \tau_e[$, where τ_a and τ_e are defined such that planes $\langle x, \theta\rangle = c\tau$ for $\tau = \tau_a$ and τ_e hit D. Changing the direction θ and intersecting stripes gives us an efficient way to reconstruct the inclusions.

By exactly the same arguments as in three dimensions, one can show that

$$\frac{1}{c}\sum_{|j|=0}^{N} \frac{a_j}{j!} \cdot b_j'(D,0;\tau) = \int_0^T \int_{\partial\Omega} \frac{\partial p}{\partial \nu}(x,t) v_\theta(x,t;\tau)\, d\sigma(x)\, dt, \tag{3.18}$$

where

$$b_j(D,t;\tau) := \int_{\mathbb{R}} \chi_D(c(\tau - t)\theta + u\theta^\perp)(c(\tau - t)\theta + u\theta^\perp - z)^j du. \tag{3.19}$$

Assuming $N = 0$ and $D = z + \epsilon B$, we can compute b_0 explicitly. We have

$$b_0(D,t;\tau) = \begin{cases} 2\sqrt{\epsilon^2 - (c|\tau - t| - \langle z, \theta\rangle)^2} & \text{if } -\epsilon < \langle z,\theta\rangle - c|\tau - t| < \epsilon, \\ 0 & \text{otherwise.} \end{cases} \tag{3.20}$$

Since $c\tau_a = \langle z,\theta\rangle - \epsilon$, $c\tau_0 = \langle z,\theta\rangle$ and $c\tau_b = \langle z,\theta\rangle + \epsilon$, we get

$$|a_0|\epsilon = \frac{c}{4}\int_{\tau_a}^{\tau_e} \left| \int_0^T \int_{\partial\Omega} \frac{\partial p}{\partial \nu}(x,t) v_\theta(x,t;\tau)\, d\sigma(x)\, dt \right| d\tau. \tag{3.21}$$

The above formula can be used to estimate $|a_0|\epsilon$.

In the case when there are m inclusions, we first compute for each l the quantity

$$\theta_{l,best} = \underset{\theta\in[0,\pi]}{\operatorname{argmax}} \left(\min_{j\neq l} |\langle z_j - z_l, \theta\rangle| \right) \tag{3.22}$$

and then, since along the direction $\theta_{l,best}$, the inclusion D_l is well separated from all the other inclusions, we can use formula (3.21) to estimate its $|a_0|\epsilon$.

To conclude this section, we make a few remarks. We first emphasize that probe functions other than those in (3.4) and (3.17) can be used.

If the medium contains small acoustic anomalies, then the effect of the inhomogeneity of acoustic speed can be neglected when the anomalies are away from the optical absorbing domains. However, we need to correct this effect when the anomalies are close to or on the absorbing region. In this case, the probe function v_y has to be corrected and this correction can be constructed by using the inner expansions derived in [7]. See also [4].

Let us digress a little to the problem posed in the free space. Let Ω be a large domain containing the support D of the nonzero absorption. We can check from the explicit formula (2.6) for p that

$$\int_0^T \int_{\partial\Omega} \left(\frac{\partial p}{\partial \nu}(x,t) v_y(x,t;\tau) - p(x,t) \frac{\partial v_y}{\partial \nu}(x,t;\tau) \right) d\sigma(x)\, dt$$
$$= \frac{1}{4\pi} \sum_{|j|=0}^{N} \frac{a_j}{j!} \cdot (b_j(D,0;\tau) - \tau b_j'(D,0;\tau)),$$

which shows the consistency of our approach with the free space problem.

4 Back-Propagation of the Acoustic Signals

If we separate out the time dependence of p, the solution to (2.2)-(2.4), by expanding $p(x,t)$ into a set of harmonic modes, then, for a given frequency ζ, the harmonic mode $\hat{p}(x,\zeta)$ satisfies the following Helmholtz equation:

$$-(\zeta^2 + c^2\Delta)\hat{p}(x,\zeta) = i\zeta(\sum_{l=1}^{m} \chi_{D_l} A_l(x)) \quad \text{in } \Omega, \tag{4.1}$$

with the boundary condition

$$\hat{p} = 0 \quad \text{or} \quad \frac{\partial \hat{p}}{\partial \nu} = 0 \quad \text{on } \partial\Omega.$$

Suppose that $-\zeta^2/c^2$ is not an eigenvalue of Δ in Ω with the Dirichlet or the Neumann boundary condition. The inverse problem we consider in this section is to reconstruct $A = \sum_{l=1}^{m} \chi_{D_l} A_l$ from the measurements of $\frac{\partial \hat{p}}{\partial \nu}$ or $\hat{p}$ on $\partial\Omega$.

In this section, we show the focusing properties of the back-propagated acoustic signals. For doing so, let $\Gamma_y(x)$, for $y \in \mathbb{R}^d \setminus \overline{\Omega}$, be the fundamental outgoing solution of $-(\zeta^2 + c^2\Delta)$ in $\mathbb{R}^d$, *i.e.*,

$$-(\zeta^2 + c^2\Delta_x)\Gamma_y(x) = \delta_{x=y}$$

subject to the outgoing radiation condition. It then follows from the divergence theorem that

$$i\zeta \sum_{l=1}^{m} \int_{D_l} A_l(x)\Gamma_y(x)dx = c^2 \int_{\partial\Omega} \hat{p}(x,\zeta) \frac{\partial \Gamma_y}{\partial \nu}(x) d\sigma(x) - c^2 \int_{\partial\Omega} \frac{\partial \hat{p}}{\partial \nu_x}(x,\zeta)\Gamma_y(x)\, d\sigma(x).$$

As before, suppose that $D_l = z_l + \epsilon B_l$, where ϵ is small. Then, we have

$$i\zeta \sum_{l=1}^{m} |D_l| A_l(z_l)\Gamma_y(z_l) \approx \begin{cases} c^2 \displaystyle\int_{\partial\Omega} \hat{p}(x,\zeta) \frac{\partial \Gamma_y}{\partial \nu}(x) d\sigma(x) & \text{if } \dfrac{\partial \hat{p}}{\partial \nu} = 0 \quad \text{on } \partial\Omega, \\ -c^2 \displaystyle\int_{\partial\Omega} \frac{\partial \hat{p}}{\partial \nu}(x,\zeta)\Gamma_y(x)\, d\sigma(x) & \text{if } \hat{p} = 0 \quad \text{on } \partial\Omega. \end{cases} \tag{4.2}$$

For R large enough, let $S_R := \{|y| = R\}$. Set

$$H(y) := -\frac{ic^2}{\zeta} \times \begin{cases} \displaystyle\int_{\partial\Omega} \hat{p}(x,\zeta)\frac{\partial\Gamma_y}{\partial\nu}(x)d\sigma(x) & \text{if } \dfrac{\partial\hat{p}}{\partial\nu} = 0 \quad \text{on } \partial\Omega, \\ \displaystyle -\int_{\partial\Omega} \frac{\partial\hat{p}}{\partial\nu}(x,\zeta)\Gamma_y(x)\,d\sigma(x) & \text{if } \hat{p} = 0 \quad \text{on } \partial\Omega, \end{cases} \tag{4.3}$$

and $\alpha_l = |D_l|A_l(z_l)$. Note that, for any $y \in \mathbb{R}^d \setminus \overline{\Omega}$, the function $H(y)$ can be computed from the boundary measurements of p.

Back-propagating p corresponds to computing

$$W(z) := \int_{S_R} \left[\frac{\partial\Gamma_z}{\partial\nu}(y)\overline{H}(y) - \frac{\partial\overline{H}}{\partial\nu}(y)\Gamma_z(y)\right] d\sigma(y), \quad z \in \Omega, \tag{4.4}$$

where H is defined in (4.3) (see e.g. [4]). Since from (4.2)

$$H(y) \approx \sum_{l=1}^{m} \alpha_l \Gamma_y(z_l)$$

for y in a neighborhood of S_R, we have

$$W(z) \approx \sum_{l=1}^{m} \overline{\alpha_l} \int_{S_R} \left[\frac{\partial\Gamma_z}{\partial\nu}(y)\overline{\Gamma_{z_l}}(y) - \frac{\partial\overline{\Gamma_{z_l}}}{\partial\nu}(y)\Gamma_z(y)\right] d\sigma(y) = 2\sum_{l=1}^{m} \overline{\alpha_l}\Im m\Gamma_{z_l}(z). \tag{4.5}$$

Thus it is now easy to find the locations z_l, $l = 1, \ldots, m$, as the points where the functional W has its maximum. Equation (4.5) shows that the reversed signal focuses on the locations of the absorbers with a resolution determined by the behavior of the imaginary part of the Green function.

5 Selective Detection

The purpose of selective detection is to focus high-intensity ultrasound towards a targeted optical absorber in biological tissue, based on the back-propagation of photo-acoustic waves generated by this optical absorber [16]. The main difficulty in focusing towards a targeted optical absorber is that photo-acoustic waves are generated by other optical absorbers in the medium as well. In this section we propose two methods of different nature to overcome this difficulty.

5.1 Multiple Signal Classification Algorithm

Here, we use the same notation as in Section 4. Suppose that for some l_0, D_{l_0} is a targeted optical absorber and its coefficient α_{l_0} is known. However, its location z_{l_0} is not known. Suppose also that

$$|\alpha_{l_0}| \geq C, \quad |\alpha_{l_0} - \alpha_l| \geq C, \quad \forall\, l \neq l_0, \tag{5.1}$$

for some positive constant C. This means that α_{l_0} is significantly different from the coefficients associated with all the other absorbers in the medium. The locations and the α_l's of all the other absorbing inclusions (D_l for $l \neq l_0$) are not known.

To localize the absorbing object D_{l_0} without knowing any of the others, we compute the following quantity for $z \in \Omega$:

$$W_{l_0}(z) := \frac{1}{\overline{\alpha_{l_0}} - 4\pi c^4 \int_{S_R} \Gamma_y(z)\overline{H}(y)\, d\sigma(y)}. \tag{5.2}$$

Let us put $k = \frac{\zeta}{c}$ for simplicity of notation. Recall that in three dimensions

$$\Gamma_y(z) = \frac{e^{ik|y-z|}}{4\pi c^2|y-z|} \approx \frac{e^{ik|y|}}{4\pi c^2|y|} e^{-ik\frac{y}{|y|}\cdot z},$$

if $|y|$ is sufficiently large while in the two-dimensional case

$$\Gamma_y(z) = \frac{i}{4c^2} H_0^{(1)}(k|y-z|) \approx \frac{e^{ik|y|+i\pi/4}}{2c^2\sqrt{2k\pi|y|}} e^{-ik\frac{y}{|y|}\cdot z}.$$

Therefore, in three dimensions we have for large R

$$\int_{S_R} \Gamma_y(z)\overline{\Gamma_y}(z_l)\, d\sigma(y) \approx \frac{1}{(4\pi R c^2)^2} \int_{S_R} e^{-ik\frac{y}{|y|}\cdot(z-z_l)}\, d\sigma(y) = \frac{1}{4\pi c^4} \frac{\sin k|z-z_l|}{k|z-z_l|},$$

and hence

$$4\pi c^4 \int_{S_R} \Gamma_y(z)\overline{H}(y)\, d\sigma(y) \approx \sum_{l=1}^{m} \overline{\alpha_l} \frac{\sin k|z-z_l|}{k|z-z_l|}.$$

This yields

$$W_{l_0}(z) \approx \frac{1}{\overline{\alpha_{l_0}} - \sum_l \overline{\alpha_l} \frac{\sin k|z-z_l|}{k|z-z_l|}}.$$

Therefore, thanks to the assumption (3.5), we have

$$W_{l_0}(z) \approx \frac{1}{\sum_{l\neq l_0} \overline{\alpha_l} \frac{\sin k|z-z_l|}{k|z-z_l|}} \gg 1 \quad \text{for } z \text{ near } z_{l_0}. \tag{5.3}$$

We also have from the assumption (5.1)

$$W_{l_0}(z) \approx \frac{1}{\overline{\alpha_{l_0}} - \sum_l \overline{\alpha_l} \frac{\sin k|z-z_l|}{k|z-z_l|}} = O(1) \quad \text{for } z \text{ away from } z_{l_0}. \tag{5.4}$$

It then follows that z_{l_0} can be detected as the point where the functional W_{l_0} has a peak. This is a MUSIC-type algorithm for locating the anomalies.

In the two-dimensional case, we compute for large R

$$\int_{S_R} \Gamma_y(z)\overline{\Gamma_y}(z_l)\, d\sigma(y) \approx \frac{1}{8k\pi Rc^4} \int_{S_R} e^{-ik\frac{y}{|y|}\cdot(z-z_l)}\, d\sigma(y) = \frac{1}{4kc^4} J_0(k|z-z_l|),$$

where J_0 is the Bessel function of the first kind of order zero. It then follows that

$$4kc^4 \int_{S_R} \Gamma_y(z)\overline{H}(y)\, d\sigma(y) \approx \sum_{l=1}^{m} \overline{\alpha_l} J_0(k|z-z_l|).$$

In two dimensions, define W_{l_0} by

$$W_{l_0}(z) := \frac{1}{\overline{\alpha_{l_0}} - 4kc^4 \int_{S_R} \Gamma_y(z)\overline{H}(y)\, d\sigma(y)}.$$

As in the three-dimensional case, the behavior of the function J_0 yields

$$W_{l_0}(z) \approx \frac{1}{\sum_{l\neq l_0} \overline{\alpha_l} J_0(k|z-z_l|)} \gg 1 \quad \text{for } z \text{ near } z_{l_0}$$

and

$$W_{l_0}(z) \approx \frac{1}{\overline{\alpha_{l_0}} - \sum_l \overline{\alpha_l} J_0(k|z-z_l|)} = O(1) \quad \text{for } z \text{ away from } z_{l_0}.$$

Therefore, exactly as in three dimensions, z_{l_0} can be detected as the point where the functional W_{l_0} has a peak.

Note that one does not need the exact value of α_{l_0}. One can get an approximation of α_{l_0} by looking numerically for the maximum of the function $F(z) = \int_{S_R} \Gamma_y(z)\bar{H}(y) d\sigma(y)$.

5.2 Multi-Frequency Approach

An alternative method for isolating the photo-acoustic signal generated by the targeted optical absorber from those generated by the others is to make use of two light pulses with slightly different excitation wavelengths, ω_1 and ω_2, tuned to the absorption spectrum of the targeted optical absorber. If the wavelengths are such that ω_1 corresponds to a low value (that can be neglected) of the absorption coefficient of the optical target and ω_2 to a high value of the absorption coefficient of the optical target, then the only difference in photo-acoustic waves generated in the medium by the two different pulses corresponds to the photo-acoustic waves generated by the light pulse selectively absorbed by the optical target (see e.g. [16, 24]). Back-propagating this signal will focus on the location of the optical target [16].

Suppose that there are two absorbers, say D_1 and D_2, and assume that

$$|D_2| \ll 1, \tag{5.5}$$

$$\mathrm{dist}(D_1, D_2) \geq C > 0, \tag{5.6}$$

which means that D_2 is small and D_1 and D_2 are apart from each other.

Let Φ_1 and Φ_2 be the light fluences corresponding respectively to illuminating the medium with excitation wavelengths ω_1 and ω_2. If we take ω_2 close to ω_1, then due to the assumptions (5.5) and (5.6) we have

$$\mu_1(x, \omega_1)\Phi_1(x) \approx \mu_1(x, \omega_2)\Phi_2(x) \quad \text{in } D_1. \tag{5.7}$$

The pressures generated by the photo-acoustic effect are given by

$$\begin{cases} \dfrac{\partial^2 p_1}{\partial t^2}(x,t) - c^2\Delta p_1(x,t) = 0, \quad x \in \Omega, \quad t \in]0,T[, \\ p_1 = 0 \quad \text{or} \quad \dfrac{\partial p_1}{\partial \nu} = 0 \quad \text{on } \partial\Omega\times]0,T[, \\ p_1|_{t=0} = \mu_1(x,\omega_1)\chi_{D_1}\Phi_1 \quad \text{and} \quad \dfrac{\partial p_1}{\partial t}\Big|_{t=0} = 0 \quad \text{in } \Omega, \end{cases}$$

and

$$\begin{cases} \dfrac{\partial^2 p_2}{\partial t^2}(x,t) - c^2\Delta p_2(x,t) = 0, \quad x \in \Omega, \quad t \in]0,T[, \\ p_2 = 0 \quad \text{or} \quad \dfrac{\partial p_2}{\partial \nu} = 0 \quad \text{on } \partial\Omega\times]0,T[, \\ p_2|_{t=0} = (\mu_1(x,\omega_2)\chi_{D_1} + \mu_2(x,\omega_2)\chi_{D_2})\Phi_2 \quad \text{and} \quad \dfrac{\partial p_2}{\partial t}\Big|_{t=0} = 0 \quad \text{in } \Omega. \end{cases}$$

For the sake of simplicity we work in the frequency domain. In view of (4.1), the difference of the generated pressures $\hat{p}_2 - \hat{p}_1$ at frequency ζ can be approximated for $x \in \Omega$ as follows:

$$(\hat{p}_2 - \hat{p}_1)(x,\zeta) \approx i\zeta|D_2|\mu_2(z,\omega_2)\Phi_2(z) \times \begin{cases} G(x,z) & \text{in the case of the Dirichlet boundary condition,} \\ N(x,z) & \text{in the case of the Neumann boundary condition,} \end{cases}$$

where G is the Dirichlet function:

$$\begin{cases} -(\zeta^2 + c^2\Delta)G(x,z) = \delta_z \quad \text{in } \Omega, \\ G = 0 \quad \text{on } \partial\Omega, \end{cases}$$

and N is the Neumann function:

$$\begin{cases} -(\zeta^2 + c^2\Delta)N(x,z) = \delta_z \quad \text{in } \Omega, \\ \dfrac{\partial N}{\partial \nu} = 0 \quad \text{on } \partial\Omega. \end{cases}$$

Here we assume that $-\zeta^2$ is not an eigenvalue of Δ in Ω with Dirichlet or Neumann boundary condition.

Define, as in (4.3), H by

$$H(y) := -\frac{ic^2}{\zeta} \begin{cases} \displaystyle\int_{\partial\Omega} (\hat{p}_2 - \hat{p}_1)(x) \frac{\partial \Gamma_y}{\partial \nu}(x) d\sigma(x) & \text{in the case of the Neumann boundary condition,} \\ \displaystyle -\int_{\partial\Omega} \frac{\partial(\hat{p}_2 - \hat{p}_1)}{\partial \nu}(x) \Gamma_y(x)\, d\sigma(x) & \text{in the case of the Dirichlet boundary condition.} \end{cases}$$

Back-propagating $\hat{p}_2 - \hat{p}_1$ yields

$$2|D_2|\mu_2(z,\omega_2)\Phi_2(z)\Im m\Gamma_z(x) \approx \int_{S_R} \left[\frac{\partial \Gamma_z}{\partial \nu}(y)\overline{H}(y) - \frac{\partial \overline{H}}{\partial \nu}(y)\Gamma_z(y) \right] d\sigma(y) \quad \text{for } x \in \Omega.$$

Here R large enough and $S_R = \{|x| = R\}$, as before. This equation shows that the reversed frequency-difference signal focus on the location z of the targeted optical absorber. Using the equation we can reconstruct the location z with a resolution given by the behavior of the imaginary part of the Green function and a signal-to-noise ratio function of the quantity $|D_2|\mu_2(z,\omega_2)\Phi_2(z)$.

6 Numerical Examples

6.1 Reconstruction Algorithm

We perform numerical simulations to validate our approach. Data used were obtained by numerically solving the 2-dimensional photo-acoustic equation (2.1) (with the Dirichlet boundary condition) with a finite-difference in time-domain method. The modelled medium was an acoustically homogeneous square (40 mm×40 mm) with $c = 1.5\text{mms}^{-1}$. The spatial step was 10 μm, and the temporal step was 9.3 ns. These steps were chosen to allow modelling the temporal Dirac in the heat function by a gaussian impulse with a full width at half maximum of 250 ns. In order to have accurate Neumann boundary data on the time interval $]0, T[$, 4000 captors (spatial step=10 μm) were aligned on each edge of the square, taking 7500 measures of $\frac{\partial p}{\partial \nu}$ over a total time length T of 70μs (time step=9.3 ns). In our further computations, derivatives were obtained using the finite difference approximation, integrals using trapezium approximation and we approximated $\int f(t)\delta(t - t_0)dt$ by the nearest discrete value of $f(t_0)$. Note also that the 7500 measures of $\frac{\partial p}{\partial \nu}$ are only used to very accurately interpolate the integral in the quantity defined by (3.8). It has been checked that using 1/1000 of the data (1/10 in time and 1/10 in each space component) still yields satisfactory reconstruction results.

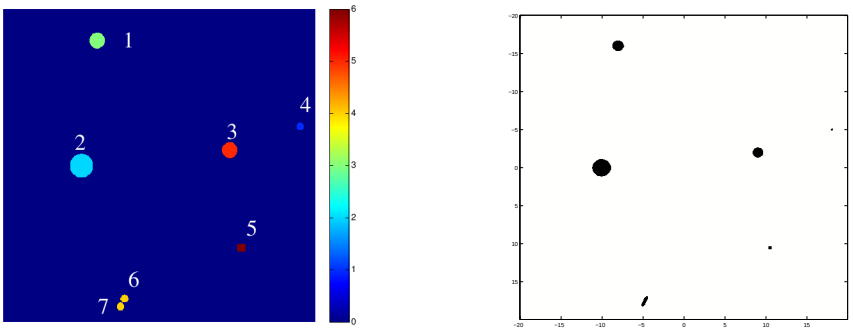

(a) Real configuration of the medium. There are seven optical inclusions.

(b) Reconstructed image of the medium. Inclusions 6 and 7 are reconstructed as a single inclusion.

Figure 1: Real and reconstructed configurations of the medium.

A first set of data was used to validate the reconstruction algorithm. Inside the medium were several unknown inclusions of various size and absorption. Initial situation is shown in Figure 1(a).

We computed the probe function for K=360 values of θ and L=800 values of τ. Then, taking the intersection of all the zero-stripes, we obtained a binary image of the medium. We also determined the gravity centers of the inclusions. Reconstructed image is shown in Figure 1(b). Gravity centers of the real and reconstructed inclusions are shown in Figure 2. First we notice our reconstruction method cannot distinguish between too close inclusions 6 and 7.

As can be observed, results are quite accurate. Not considering inclusions 6-7, mean error on the positions is less than the pixel size of our image (0.074 vs. 0.08).

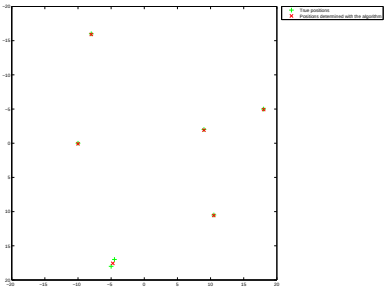

Figure 2: Gravity centers of actual and reconstructed inclusions.

6.2 Back-Propagation Algorithm

To test the back-propagation algorithm, we simulated data based on the Helmholtz equation (4.1) by using a finite element method. For all the simulations, we used frequency $\zeta = 5\text{Mrads}^{-1}$. Note that one could not use the same space-time data as in the reconstruction algorithm since the time length of these data is limited. Because one has only access to $p(x,t)$ for $t \in]0;T[$, taking the discrete Fourier transform of these data would not give $\hat{p}(x,\zeta)$, but $\hat{p}$ is acquired by convolution with the *sinc* function.

We first applied the back-propagation algorithm on data generated by 7 inclusions of radius 1mm. Each inclusion has a similar absorbed energy $a_0 = 1$. The actual configuration and the resulting image of $W(z)$ are shown in Figure 3.

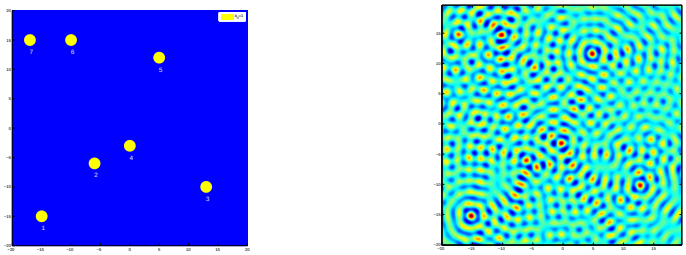

Figure 3: Back-propagation simulation. Left: Actual configuration, Right: Plot of $W(z)$.

6.3 Selective Detection

6.3.1 MUSIC Algorithm

We first tested the MUSIC algorithm on a simple situation with only one inclusion. We give the initial situation, the reconstruction function $F(z) = \int_{S_R} \Gamma_y(z)\bar{H}(y)d\sigma(y)$ which is close to the time-reversal philosophy [4], and then the MUSIC function $W_{l_0}(z)$ which has a sharp peak around the inclusion. Results are shown in Figure 4.

We then simulated data with different energies to verify that the MUSIC algorithm could selectively distinguish an inclusion whose absorbed energy is much different from any other inclusion. Results, shown in Figures 5 and 6, are quite satisfying since we could separate the contrasted inclusion among seven inclusions, even with contrast equal to 2.

6.3.2 Multi-Frequency Approach

We simulated 2 sets of data corresponding to the situation described in Section 5.2. We assumed that inclusion 6 was totally transparent at wavelength ω_1 but appeared

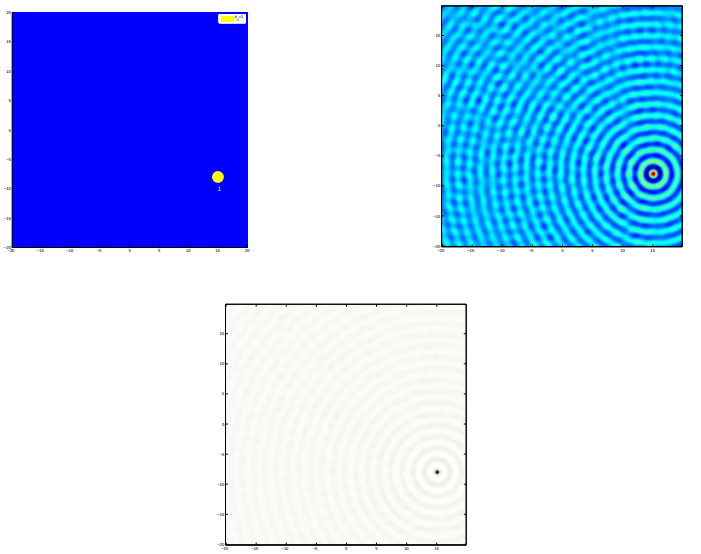

Figure 4: Selective detection: MUSIC simulation with a single inclusion. Top left: actual configuration, top right: plot of $F(z)$, bottom: plot of $W_{l_0}(z)$.

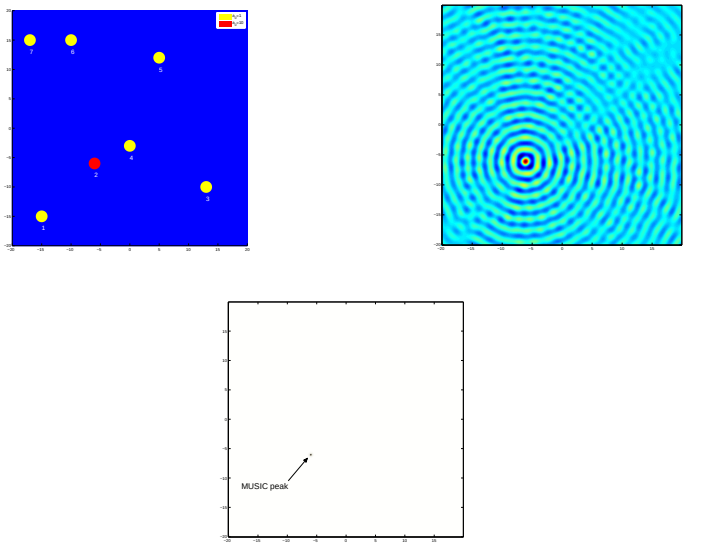

Figure 5: Selective detection: MUSIC simulation with 7 inclusions, contrast=10.

just like the other inclusions at ω_2. As expected, one can see in Figure 7 that the algorithm managed to isolate inclusion 6.

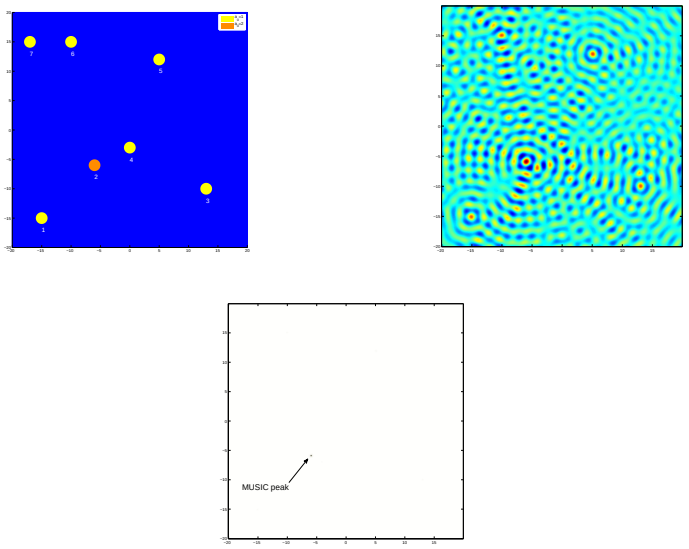

Figure 6: Selective detection: MUSIC simulation with 7 inclusions, contrast=2.

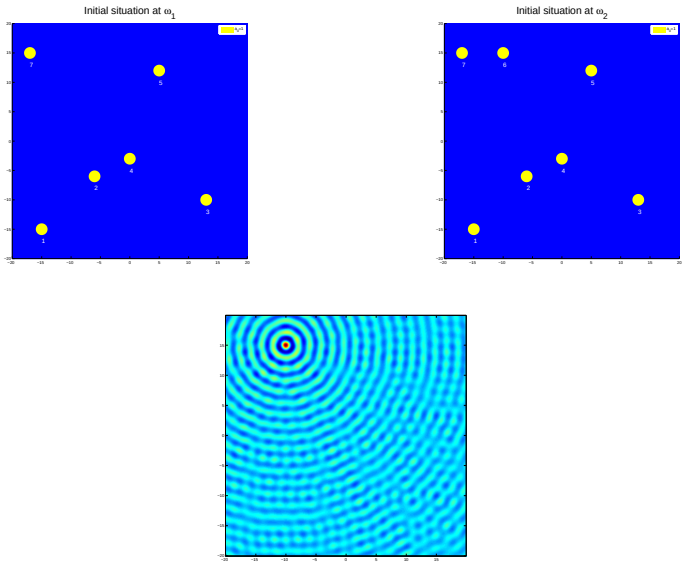

Figure 7: Selective detection: Multi-frequency approach results. Inclusion 6 is transparent at one frequency (top left), is seen at other frequency (top right), and hence is separated (bottom).

7 Concluding Remarks and Extensions

In the literature, it has been assumed in photo-acoustic tomography that ultrasound propagates in a boundary-free infinite medium. The reconstruction procedures have been based on the spherical Radon transform.

In this paper, we have provided a new method for reconstructing absorbing inclusions inside a bounded medium where boundary conditions are imposed. Because of the acoustic boundary conditions, the spherical Radon inverse transform can not be applied. Our approach is to make an appropriate averaging of the measurements by using particular solutions to the wave equation. It is related to time-reversal in the sense that it is a convolution with a reversed wave. It has been validated by numerical simulations.

In the case where the time-dependence of the induced pressure by the photo-acoustic effect can be separated out, we have designed a back-propagation algorithm to detect the absorbers. It is resolution is determined by the behavior of the imaginary part of the Green function of the acoustic medium. To isolate the photo-acoustic signal generated by a targeted optical absorber from those generated by the others we developed two different approaches: the first approach is of MUSIC-type and the second one is a multi-frequency approach. These two approaches have the same resolution.

All the algorithms designed in this paper can be extended to the case where the acoustic background medium is heterogeneous but known.

Our approach extends to the case where only a part of the boundary is accessible. If we suppose that the measurements are only done on a part Γ of the boundary $\partial\Omega$, then the detection of the absorbers from these partial measurements hold only under an extra assumption on T and Γ. The geometric control theory [8] can be used to construct an appropriate probe function in the limited-view data case. This will be discussed in a forthcoming paper. We also intend to generalize our inversion formula to the case where the medium is acoustically inhomogeneous (contains small acoustical scatterers and/or in the presence of attenuation). Using an asymptotic approach, we would derive the effect of the presence of acoustic small anomalies on the reconstruction of the optical properties and develop an algorithm that corrects the undesired effect. Another important problem is to develop a stable and accurate method for reconstructing the optical absorption coefficient from the absorbed energy. This would be also the subject of a forthcoming work.

References

[1] M. Agranovsky and P. Kuchment, Uniqueness of reconstruction and an inversion procedure for thermoacoustic and photoacoustic tomography with variable sound speed, Inverse Problems, 23 (2007), 2089-2102.

[2] M. Agranovsky, P. Kuchment, and L. Kunyansky, On reconstruction formulas and algorithms for the thermoacoustic and photoacoustic tomography, to appear in L. H. Wang (Editor) "*Photoacoustic Imaging and Spectroscopy*," CRC Press.

[3] G. Ambartsoumian and S. Patch, Thermoacoustic tomography Implementation of exact backprojection formulas, math.NA/0510638.

[4] H. Ammari, *An Introduction to Mathematics of Emerging Biomedical Imaging*, Math. & Appl., Vol. 62, Springer-Verlag, Berlin, 2008.

[5] H. Ammari, An inverse initial boundary value problem for the wave equation in the presence of imperfections of small volume, SIAM J. Control Optim., 41 (2002), 1194–1211.

[6] H. Ammari, Y. Capdeboscq, H. Kang, and A. Kozhemyak, Mathematical models and reconstruction methods in magneto-acoustic imaging, Euro. J. Appl. Math., 20 (2009), 303–317.

[7] H. Ammari, P. Garapon, L. Guadarrama Bustos, and H. Kang, Transient anomaly imaging by the acoustic radiation force, J. Diff. equat., to appear.

[8] C. Bardos, G. Lebeau, and J. Rauch, Sharp sufficient conditions for the observation, control, and stabilization of waves from the boundary, SIAM J. Control Optim., 30 (1992), 1024-1065.

[9] E. Bossy, K. Daoudi, A.-C. Boccara, M. Tanter, J.-F. Aubry, G. Montaldo, and M. Fink, Time reversal of photoacoustic waves, Appl. Phys. Lett. 89 (2006), 184108.

[10] B.T. Cox, S.R. Arridge, and P.C. Beard, Gradient-based quantitative photoacoustic image reconstruction for molecular imaging, Proc. of SPIE Vol. 6437 (2007), 64371T, doi:10.1117/12.700031.

[11] B.T. Cox, S.R. Arridge, and P.C. Beard, Photoacoustic tomography with a limited-aperture planar sensor and a reverberant cavity, Inverse Problems 23 (2007), S95-S112.

[12] A.J. Devaney, A filtered backpropagation algorithm for diffraction tomography, Ultrasonic Imaging, 4 (1982), 336–350.

[13] A.J. Devaney, Time reversal imaging of obscured targets from multistatic data, IEEE Trans. Antennas Propagat., 523 (2005), 1600–1610.

[14] M. Fink, Time-reversal acoustics, in *Inverse Problems, Multi-Scale Analysis and Homogenization,* 151–179, Contemp. Math., Vol. 408, Rhode Island, Providence, 2006.

[15] A.R. Fisher, A.J. Schissler, and J.C. Schotland, Photoacoustic effect of multiply scattered light, Phys. Rev. E, 76 (2007), 036604.

[16] A. Funke, J-F. Aubry, M. Fink, A-C. Boccara, E. Bossy, Photoacoustic guidance of high intensity focused ultrasound with selective optical contrasts and time-reveral, Appl. Phys. Lett. 94 (2009), *in press.*

[17] F.G. Friedlander, *The Wave Equation on a Curved Space-Time*, Cambridge University Press, Cambridge, 1975.

[18] M. Haltmeier, T. Schuster, and O. Scherzer, Filtered backprojection for thermoacoustic computed tomography in spherical geometry, Math. Meth. Appl. Sci., 28 (2005), 1919-1937.

[19] M. Haltmeier, O. Scherzer, P. Burgholzer, R. Nuster, and G. Paltauf, Thermoacoustic tomography and the circular Radon transform: exact inversion formula, Math. Model. Meth. Appl. Sci., 17(4) (2007), 635-655.

[20] F. Hetch, O. Pironneau, K. Ohtsuka and A. Le Hyaric, FreeFem++, http://www.freefem.org, 2007.

[21] P. Kuchment and L. Kunyansky, Mathematics of thermoacoustic tomography, European J. Appl. Math., 19 (2008), 191–224.

[22] S.K. Patch and O. Scherzer, Guest editors' introduction: Photo- and thermoacoustic imaging, Inverse Problems 23 (2007), S1–10.

[23] J. Ripoll and V. Ntziachristos, Quantitative point source photoacoustic inversion formulas for scattering and absorbing media, Phys. Rev. E, 71 (2005), 031912.

[24] Y.W. Wang, X.Y. Xie, X.D. Wang, G. Ku, K.L. Gill, D.P. O'Neal, G. Stoica, and L.V. Wang, Photoacoustic tomography of a nanoshell contrast agent in the in vivo rat brain, Nano Letters, 4 (2004), 1689–1692.

[25] L.V. Wang and X. Yang, Boundary conditions in photoacoustic tomography and image reconstruction, J. Biomed. Optics, 12 (2007), 014027.

[26] M. Xu and L.V. Wang, Photoacoustic imaging in biomedicine, Review of Scientific Instruments 77, 041101, 2006.

[27] Y. Xu, L.V. Wang, G. Ambartsoumian, and P. Kuchment, Reconstructions in limited view thermoacoustic tomography, Medical Physics 31 (2004), 724–733.

[28] Z. Yuan, C. Wu, H. Zhao, and H. Jiang, Imaging of small nanoparticle-containing objects by finite-element-based photoacoustic tomography, Optics Lett. 30 (2005), 3054–3056.